Shading correction algorithm for cone-beam CT in radiotherapy: Extensive clinical validation of image quality improvement

K D Joshi[a], T E Marchant[b, a], and C J Moore[b, a]

[a]Christie Medical Physics and Engineering, The Christie NHS Foundation Trust, Manchester, M20 4BX, UK.
[b]The University of Manchester, Manchester Academic Health Science Centre, The Christie NHS Foundation Trust, Manchester, M20 4BX, UK.

ABSTRACT

A shading correction algorithm for the improvement of cone-beam CT (CBCT) images (*Phys. Med. Biol.* **53** 5719–33) has been further developed, optimised and validated extensively using 135 clinical CBCT images of patients undergoing radiotherapy treatment of the pelvis, lungs and head & neck. An automated technique has been developed to efficiently analyse the large number of clinical images. Small regions of similar tissue (for example fat tissue) are automatically identified using CT images. The same regions on the corresponding CBCT image are analysed to ensure that they do not contain pixels representing multiple types of tissue. The mean value of all selected pixels and the non-uniformity, defined as the median absolute deviation of the mean values in each small region, are calculated. Comparisons between CT and raw and corrected CBCT images are then made. Analysis of fat regions in pelvis images shows an average difference in mean pixel value between CT and CBCT of 136.0 HU in raw CBCT images, which is reduced to 2.0 HU after the application of the shading correction algorithm. The average difference in non-uniformity of fat pixels is reduced from 33.7 in raw CBCT to 2.8 in *shading-corrected* CBCT images. Similar results are obtained in the analysis of lung and head & neck images.

Keywords: CLIN (clinical evaluation), CTCB (cone-beam CT), ONC (oncology)

This paper was presented at SPIE Medical Imaging 2017:

K Joshi, T Marchant, C Moore, "Shading correction for cone-beam CT in radiotherapy: Extensive clinical validation of image quality improvement," Medical Imaging 2017: Physics of Medical Imaging, Proc. SPIE 10132, 101322A (2017).

http://dx.doi.org/10.1117/12.2254035

1. INTRODUCTION

Cone beam CT (CBCT) imaging[1,2] has become an integral part of modern radiotherapy. With the ability to acquire images of patients at the time of treatment, CBCT imaging has allowed image guided radiotherapy (IGRT)[3] to become standard practice.

CBCT images are typically of sufficient quality to allow patients to be set up for treatment accurately, by examining bony anatomy and the position of target structures[4]. However, CBCT images often exhibit a range of artefacts that degrade their quality. These are caused by a number of effects, including the increased amounts of scatter resulting from the cone-shaped beam of x-rays. The pixel values in the images do not accurately represent Hounsfield Units (HU), and the images can exhibit poor uniformity – pixels representing a particular

Corresponding author: kiran.joshi@christie.nhs.uk

type of tissue can have different values depending on their location in the images. This is illustrated in Figure 1, which shows a single slice of a pelvis CBCT image volume (a) and a corresponding CT image (b) of the same patient. Due to these artefacts, CBCT images cannot be used, for example, to calculate the dose delivered by a radiotherapy treatment plan[5].

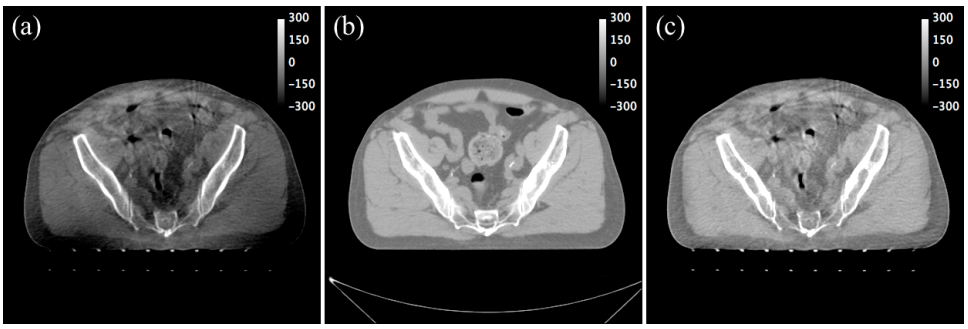

Figure 1. Example slices of CBCT and CT image volumes of a pelvis. (a) shows a raw CBCT image volume after being acquired and reconstructed using the Elekta XVI system. (b) shows a CT image of the same patient, acquired some time before the CBCT image. (c) shows the image in panel (a) after it has been processed using our shading correction algorithm.

Many methods have been studied that aim to improve the quality of CBCT images. For example: alterations to the imaging system hardware, such as anti-scatter grids[6] and beam filters[7,8]; scatter corrections applied to the CBCT projection images before reconstruction[9,10]; assignment of uniform densities to different regions of the CBCT images[5,13]; and derivations of calibration curves based on phantom measurements or site-specific population averages[14,15]. Deformable image registration is also being investigated as a technique for mapping regions of a planning CT image to a corresponding CBCT image[16,17].

In a previous work[18] we described a post-processing algorithm that uses a corresponding radiotherapy planning CT image to derive a low spatial frequency greyscale shading map that is used to correct CBCT images. The result of processing the image in Figure 1(a) with our algorithm is shown in Figure 1(c), and will be referred to as a *shading-corrected* CBCT image. The shading correction algorithm greatly improves both the overall HU calibration and uniformity of CBCT images.

In this work we have optimised and refined the shading correction algorithm, and have performed an extensive validation of the technique by analysing the greyscale values of 135 *shading-corrected* CBCT images of pelvis, lung and head & neck radiotherapy patients. Both the shading-correction algorithm and greyscale analysis have been fully automated to enable the efficient processing of large numbers of clinical images.

2. METHODS AND MATERIALS

2.1 Image and treatment plan data

CT and CBCT images were selected from patients that have undergone radiotherapy treatment of the pelvis, lungs or head & neck. Fifteen patients for each site and three CBCT images per patient were chosen, providing 45 CBCT images per site — 135 in total — to test and validate the shading correction algorithm. All images were anonymised prior to processing and analysis.

CT images were acquired using Siemens Somatom Definition AS and Philips Brilliance Big Bore CT scanners. CBCT images were acquired using the Elekta XVI imaging system (XVI software versions 4.5 & 5, Elekta, Crawley, UK).

2.2 CBCT shading correction algorithm

In a previous work[18] we documented the initial version of the CBCT shading correction algorithm. A summary of the processing steps is also given here for completeness. A comparison between the CBCT and the corresponding planning CT image is used as the basis for the correction. A global linear scaling of the CBCT image voxels

is first applied to produce a CBCT image volume with voxel values corresponding approximately to HU. The scaling is derived by analysis of the CT and CBCT image histograms. The CBCT image histogram is linearly scaled until it more closely resembles the histogram of the CT image. A shading map is then produced by taking the ratio of the CT and *histogram-scaled* CBCT images. Regions of the CBCT and CT images that are not directly comparable — e.g. regions of gas in the rectum — are taken into account in the correction algorithm by creating masks that identify any image data that may be missing in one of the images. The shading map is smoothed so that it corrects for low spatial frequency brightness variations in the CBCT image.

Several modifications have been made to the algorithm in order to improve its speed and robustness, as well as to enable the efficient processing of lung images. The algorithm has been completely reimplemented in `C++` and makes use of the Insight Toolkit (ITK)[19]. In some places, where further speed increases were necessary, image processing functions were rewritten from scratch. For example an efficient implementation of three dimensional binary morphology was produced; the time required to perform a three dimensional erosion or dilation was reduced from around $1 - 2$ s per image volume to less than 0.05 s per image volume[20].

The shading-correction algorithm is completely automated, requiring no user interaction after the initial CT and CBCT images have been selected. In order to minimise the time burden placed on potential radiotherapy physicists using the correction algorithm, the processing time required has been reduced as much as possible. At the time of publishing it is possible to apply the entire correction procedure to a full CBCT image volume in around five seconds.

2.3 Image quality analysis

CBCT image quality is estimated by defining regions of a known tissue type using a CT image, and calculating the mean and standard deviation of the pixel greyscale values inside the same regions on the corresponding CBCT images. Regions of fat tissue are defined as having pixels with values in the range -100 – 0 HU, and regions of higher density tissue, referred to simply as *muscle*, are defined as those with pixel values in the range 0 – 150 HU.

When analysing lung images, regions of lung tissue are not identified and compared. There is significant local anatomical variation within the lungs, with spongy tissue having different density to blood vessels and bronchi. In Figure 2(a) profiles are taken through a region of fat and lung tissue in a CT image of a lung patient. The difference between the pixel value at each point along the profile and the mean value is shown in Figure 2(b). Differences of up to 200 HU are visible in small regions in the profile through the lung tissue. The profile through the fat tissue, however, shows that the pixel values are much more consistent.

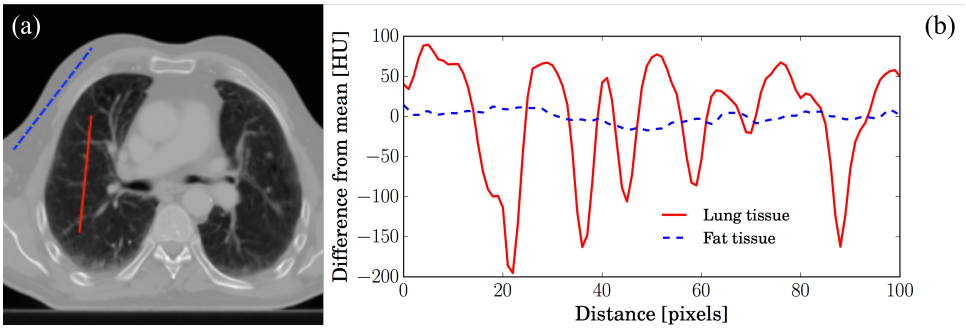

Figure 2. Example profiles through a lung CT image. (a) shows the location of two profiles, taken through fat tissue (blue, dashed) and lung tissue (red, solid). (b) shows the difference between the pixel value at each point along the profile and the mean value of pixels along the profile.

It is therefore not expected that small regions of lung tissue would be similar throughout a CT image, nor between a CT and CBCT image, and would not provide a reliable test of the image quality.

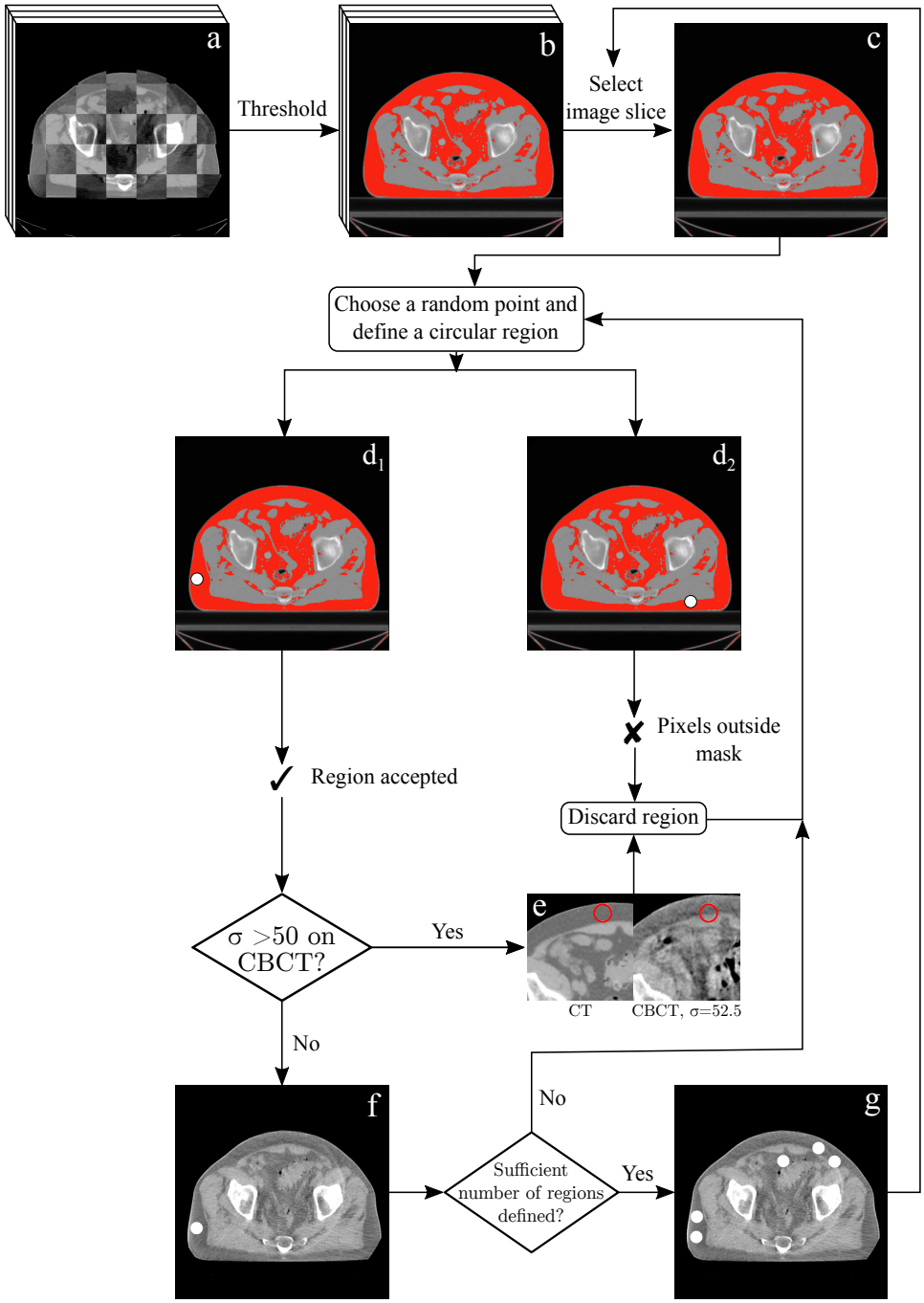

Figure 3. Illustration of the automated method used to assess CBCT image quality.

2.3.1 Automated analysis method

Due to the large number of clinical images studied, an automated method for defining and analysing regions of similar tissue was developed. The analysis workflow is illustrated in Figure 3.

The first step of the automated analysis is to register the CT image to the corresponding CBCT image. The registration is performed as part of the shading correction algorithm, so the same transformation is applied to the CT image here. A checkerboard comparison of the CT and CBCT images after registration is shown in Figure 3(a). Pixels representing a particular type of tissue in the CT image volume are then selected by applying a threshold. An example of the resulting mask is shown in Figure 3(b), with areas of fat tissue highlighted in red. A single slice of the image volume is then selected (Figure 3(c)). A random point in the slice is chosen and all pixels within a circle of radius R, centred on the point, are selected. All of the selected pixels inside the circular region must lie inside the tissue mask (Figure 3(d_1)). If any pixels lie outside the mask (Figure 3(d_2)), the region is discarded and another starting point is selected. The region radius R is varied as the analysis progresses. Initially the algorithm searches for large regions ($R = 12$) however if no suitable region can be found after 5000 attempts, the region radius is reduced by 1 and the process is repeated. A strategy such as this is required in order to locate, for example, regions of fat in images of the head, where there is often very little fat tissue.

Anatomical changes to the patient are expected to have taken place between the acquisition of the CT and CBCT images. Therefore it is possible that the region defined using the CT image will not contain the same tissue type when transposed to the CBCT image. In order to mitigate this potential problem the region is only accepted if the pixel values inside the region on the *shading-corrected CBCT image* have standard deviation less than 50 (Figure 3(e)). Once a suitable region has been identified (Figure 3(f)) the processes is repeated until a sufficient number of regions have been defined on the slice (Figure 3(g)). Five regions per slice are defined in the analysis presented below. The next slice of the CT image volume is then selected and the processes is repeated until circular regions have been found on all slices of the image.

A standard deviation of 50 was found empirically to be sufficient to determine when a circular region contained pixels of more than one type of tissue in the *shading-corrected* CBCT images. Figure 4 shows examples of circular regions that are rejected by imposing this requirement.

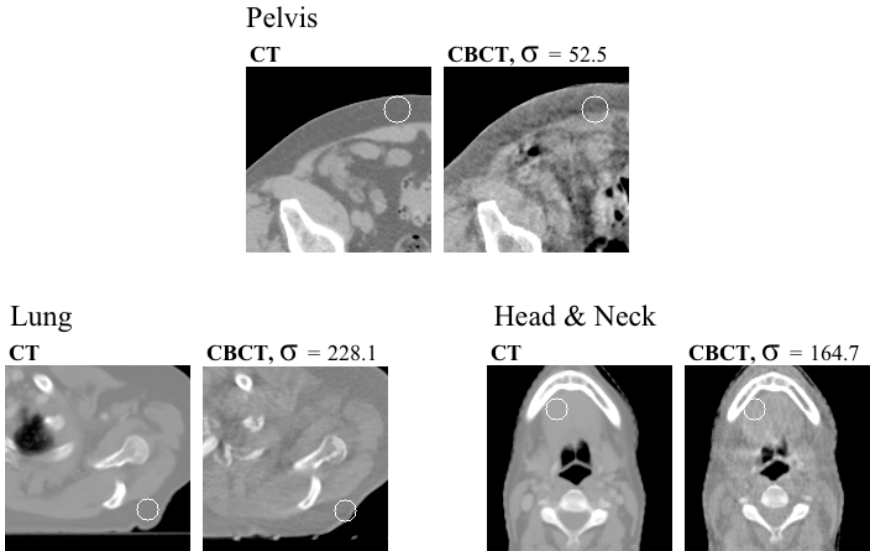

Figure 4. Examples of circular regions, defined automatically using CT images, which are rejected by requiring that pixel values in the corresponding *shading-corrected* CBCT have standard deviation less than 50. In the pelvis image, differences in the distribution of fat tissue in the CBCT image cause the region to contain both fat and muscle. The lung images show a patient whose distribution of fat tissue has changed due to weight loss or a change in arm position; a region containing fat in the CT image also contains pixels representing air in the CBCT image, resulting in the pixel values having a large standard deviation. Slight differences in the position of the patient's jaw in the head & neck image results in the circular region on the CBCT image containing some bone pixels.

In order to investigate the effects of the different parts of the correction algorithm, the CBCT images are analysed after they have been partially and fully corrected. CBCT images analysed after only the global linear scaling of the pixel values has been applied are referred to as *histogram-scaled*. Images that have been processed using the full shading correction algorithm are referred to as *shading-corrected*.

The quality of the CBCT images is then estimated by taking the difference between the mean value of the pixels in the regions defined on the CT image, and that calculated using the CBCT images. A non-zero difference in mean pixel value would indicate that the CBCT image pixels do not accurately represent Hounsfield Units. For each image we also define the *non-uniformity* as the *median absolute deviation*[21] of the means of the pixel values in each region. If all of the regions in an image had exactly the same mean value, the *non-uniformity* would be zero. A non-zero *difference* in non-uniformity indicates that a CBCT image is more non-uniform than the corresponding CT image – the pixels representing a particular type of tissue have a range of values depending on their location in the image.

3. RESULTS AND DISCUSSION

3.1 Pelvis images

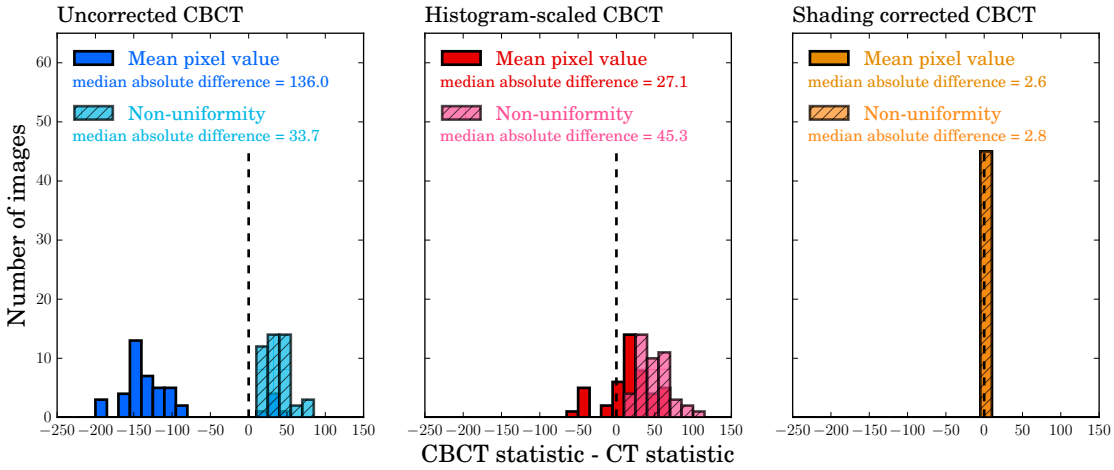

Figure 5. Differences between the mean value (dark histograms) and non-uniformity (light histograms) of pixels representing fat tissue in pelvis CT images, and those in corresponding uncorrected CBCT (left), *histogram-scaled* CBCT (middle) and *shading-corrected* CBCT (right) images.

Results of the analysis of fat and muscle regions in pelvis images are shown in Figure 5 and Figure 6 respectively. Analysis of the two regions show consistent results. The uncorrected CBCT images exhibit differences in mean pixel value of around -130 in regions of fat and around -220 in regions of muscle tissue. There are a small number of images that show a much smaller difference in mean pixel value. These pelvis images were acquired using an updated version of the Elekta XVI software (XVI 5.0) and are discussed in Appendix A. The non-uniformity of the pixels in the fat (muscle) regions is around 30 (20), indicating the non-uniformity in the images; the pixels representing fat and muscle in the CBCT images do not all have similar values, as is the case in the corresponding CT images.

After applying the global linear scaling to the images (red histograms) the differences in mean pixel value are closer to zero, indicating that the pixels of the histogram-scaled CBCT images more closely resemble the Hounsfield Units present in the CT images. The non-uniformity of the pixel values are largely unchanged; a simple global linear scaling of pixel values does not, by definition, correct for non-uniformities in the CBCT image.

Once the full shading correction has been applied the differences in mean pixel value and non-uniformity are very close to zero. All regions of similar tissue in the shading-corrected CBCT images contain approximately the same pixel value, and the value is close to what is calculated using the corresponding CT image.

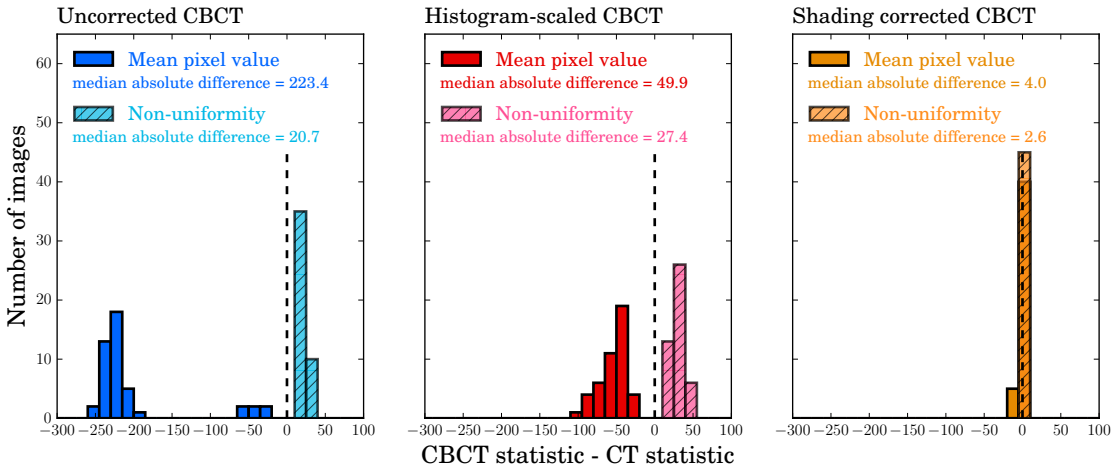

Figure 6. Differences between the mean value (dark histograms) and non-uniformity (light histograms) of pixels representing muscle tissue in pelvis CT images, and those in corresponding uncorrected CBCT (left), *histogram-scaled* CBCT (middle) and *shading-corrected* CBCT (right) images.

3.2 Lung images

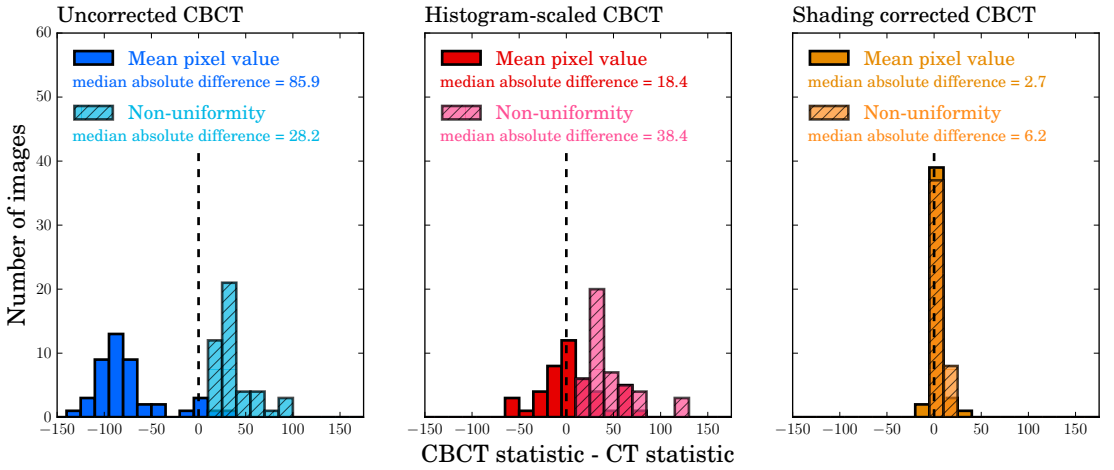

Figure 7. Differences between the mean value (dark histograms) and non-uniformity (light histograms) of pixels representing fat tissue in lung CT images, and those in corresponding uncorrected CBCT (left), *histogram-scaled* CBCT (middle) and *shading-corrected* CBCT (right) images.

Results of the greyscale analysis of lung images are shown in Figure 7 and Figure 8. The results are qualitatively the same as those of the pelvis images: the uncorrected CBCT images have regions of fat and muscle tissue with pixel values significantly different from those in the corresponding CT images; applying the histogram scaling part of the shading correction algorithm reduces the difference in the mean pixel values but does not reduce the non-uniformity of the pixel values; the full shading correction further reduces the difference in mean pixel value and significantly improves the uniformity of the CBCT images.

3.3 Head & neck images

Figures 9, 10 show the results of the automated greyscale analysis on the clinical head & neck images.

The head & neck results are similar to those from the pelvis and lung images. A feature of the histograms that should be noted is that the histogram-scaling part of the algorithm appears to have little effect on the quality of the CBCT images (i.e. red and blue histograms are very similar). It is only after the full shading

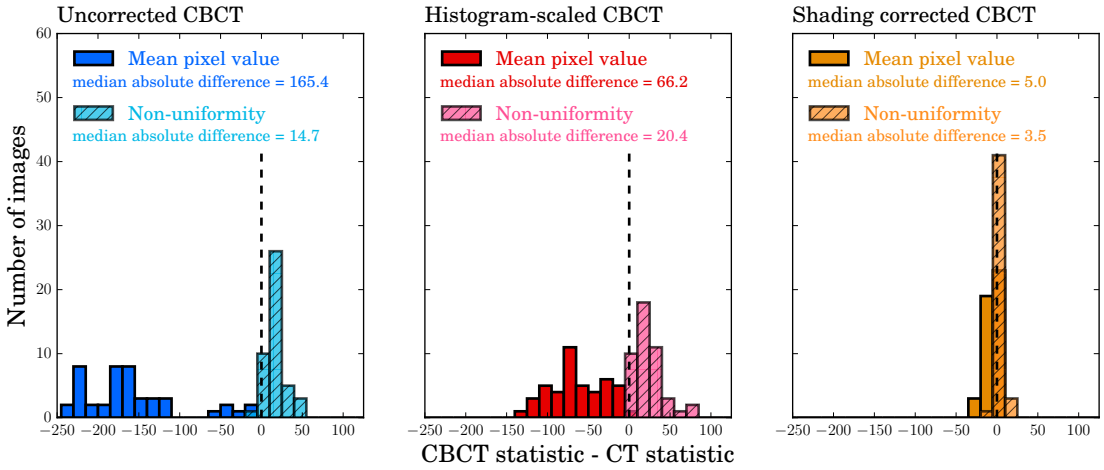

Figure 8. Differences between the mean value (dark histograms) and non-uniformity (light histograms) of pixels representing muscle tissue in lung CT images, and those in corresponding uncorrected CBCT (left), *histogram-scaled* CBCT (middle) and *shading-corrected* CBCT (right) images.

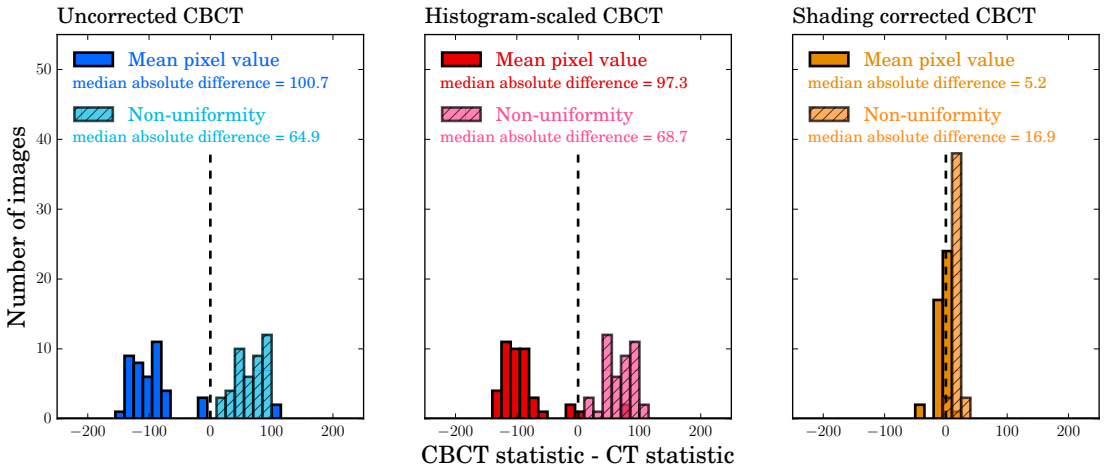

Figure 9. Differences between the mean value (dark histograms) and non-uniformity (light histograms) of of pixels representing regions of fat tissue calculated using head & neck CT images, and those calculated with corresponding uncorrected CBCT (left), histogram-scaled CBCT (middle) and shading-corrected CBCT (right) images.

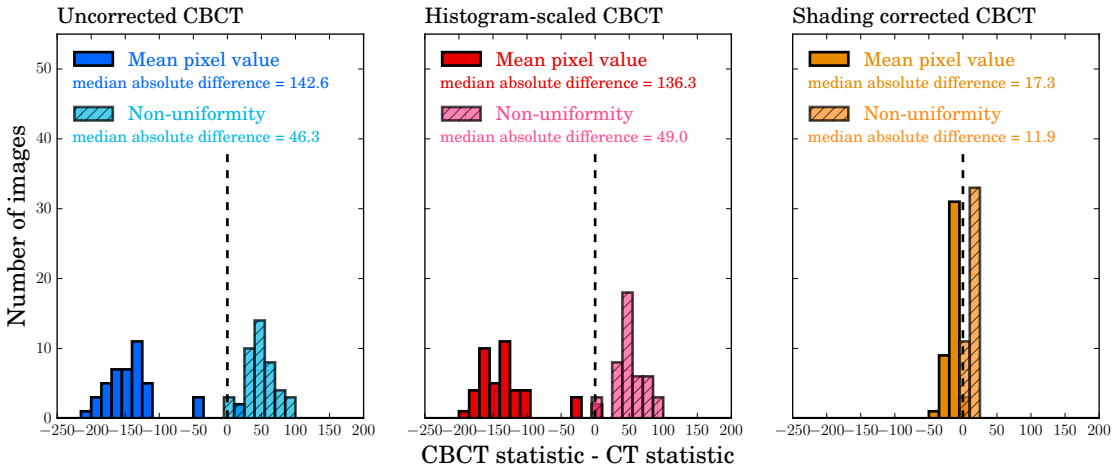

Figure 10. Differences between the mean value (dark histograms) and non-uniformity (light histograms) of of pixels representing regions of muscle tissue calculated using head & neck CT images, and those calculated with corresponding uncorrected CBCT (left), histogram-scaled CBCT (middle) and shading-corrected CBCT (right) images.

correction is applied that a significant improvement in image quality is made. The reason for this is the same as for the small number of uncorrected pelvis images that show only a slight difference in mean pixel value; the majority of the clinical head & neck images that were collected had been acquired with a more recent version of the Elekta XVI software (XVI 5.0). Some observations about the images acquired with different versions of the XVI software are presented in Appendix A.

3.4 Discussion

The results of running the shading correction algorithm on a large number of clinical images, across a range of imaging sites, demonstrate the clear improvement in image quality that is provided on top of a simple correction such as a global linear scaling of the pixel values. The *shading-corrected* CBCT images contain pixel values that more closely resemble Hounsfield Units than their uncorrected counterparts, and the uniformity of pixels representing particular types of tissue is greatly improved.

It was previously noted that some uncorrected pelvis images acquired with an updated version of the XVI software (XVI 5.0) had a much smaller difference in mean pixel value – differences of around 50 HU compared to around 225 HU. However the head & neck images, which were also acquired with XVI 5.0, exhibit reasonably large differences in mean pixel value between CT and uncorrected CBCT of around 100 – 150 HU. The reason for this is that images of head & neck patients are typically acquired using a small field of view, which does not encompass the full patient outline the level of the shoulders. CBCT images can therefore suffer from large artefacts around the level of the shoulders, as illustrated in Figure 11.

Table 1: Median absolute difference in mean fat tissue pixel value between CT and uncorrected/corrected CBCT images. Regions of fat tissue are split into three groups according to their longitudinal position, illustrated in Figure 11 (b).

longitudinal group	uncorrected CBCT median abs. diff.	corrected CBCT median abs.diff
1 - 'low'	255	18
2 - 'medium'	46	3
3 - 'high'	15	5

It is therefore the regions of fat and muscle tissue defined in approximately the inferior third of a head & neck image that lead to the relatively large median absolute difference in mean fat tissue pixel value between CT and uncorrected CBCT (Figure 9). This can be confirmed by splitting the analysis of regions of fat tissue into three groups according to their longitudinal position, illustrated with blue lines and numbers on Figure 11 (b). Median absolute differences in mean fat tissue pixel values between CT and (un)corrected CBCT images are summarised in Table 1.

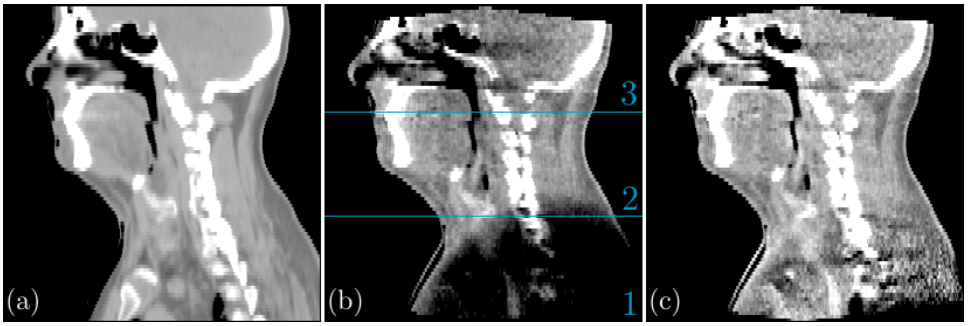

Figure 11. Saggital slice of (a) CT, (b) uncorrected CBCT and (c) *shading-corrected* CBCT images of a head & neck patient. Due to the small field of view used to acquire the uncorrected CBCT image, significant artefacts can be seen at the level of the shoulders. The shading correction algorithm removes these artefacts to a large extent. The quality of the uncorrected CBCT image above the level of the shoulders is good and is not significantly affected by the shading correction algorithm.

Although effort has been made to ensure that pixels representing the same type of tissue are compared on the CT and CBCT images, the nature of a fully automated validation technique means that this may not always be the case. The results presented here can therefore be considered as giving a conservative estimate of the performance of the shading correction algorithm; a difference in mean pixel value and non-uniformity would only be made larger by selecting pixels of a different tissue type. It would not be possible for a poorly-corrected CBCT image to appear to be of similar quality as a CT image using the analysis presented here.

An alternative method for determining whether the processed CBCT images are of sufficient quality for use in a clinical environment would be to perform dose recalculations using the corrected CBCT images. A study assessing the dosimetric impact of the shading correction has also been performed[22].

The results suggest that the current implementation of the shading correction algorithm is robust and reliable enough to be tested in a clinical environment with no user intervention. The automated greyscale analysis produces consistent results, and could be adapted for use as a fast on-line check that the shading correction algorithm has functioned correctly.

4. CONCLUSIONS

A post-processing method for the enhancement of CBCT images[18], has been optimised and refined to increase robustness and reduce required processing time. The shading correction algorithm runs without any user interaction and can produce enhanced CBCT image volumes in around 5 seconds. The algorithm has been tested and validated extensively using a 135 clinical images of patients undergoing radiotherapy of the pelvis, lung and head & neck.

An automated method has been developed for assessing the quality of the processed CBCT images. Regions of fat and muscle tissue are automatically selected using CT images. Mean pixel values inside the regions are calculated and compared to the values calculated using the same regions on the corresponding CBCT images. Results confirm that the corrected CBCT images are of better quality that the unprocessed versions, and that the shading correction algorithm is robust and effective. A further study assessing the dosimetric impact of the shading correction has also been performed[22].

Acknowledgments

This work was supported by the UK Medical Research Council (MRC) grant No. MR/L023059/1.

References

[1] Jaffray, D. A., Siewerdsen, J. H., Wong, J. W., Martinez, A. A., "Flat-panel cone-beam computed tomography for image-guided radiation therapy," International Journal of Radiation Oncology*Biology*Physics **53**(5), 1337–1349 (2002).

[2] Letourneau, D., Wong, J. W., Oldham, M., Gulam, M., Watt, L., Jaffray, D. A., Siewerdsen, J. H., Martinez, A. A., "Cone-beam-CT guided radiation therapy: technical implementation," Radiotherapy and Oncology **75**(3), 279–286 (2005).

[3] McBain, C. A., Henry, A. M., Sykes, J., Amer, A., Marchant, T., Moore, C. M., Davies, J., Stratford, J., McCarthy, C., et al., "X-ray volumetric imaging in image-guided radiotherapy: The new standard in on-treatment imaging," International Journal of Radiation Oncology*Biology*Physics **64**(2), 625–634 (2006).

[4] Guckenberger, M., Meyer, J., Vordermark, D., Baier, K., Wilbert, J., Flentje, M., "Magnitude and clinical relevance of translational and rotational patient setup errors: A cone-beam CT study," International Journal of Radiation Oncology*Biology*Physics **65**(3), 934–942 (2006).

[5] Fotina, I., Hopfgartner, J., Stock, M., Steininger, T., Ltgendorf-Caucig, C., Georg, D., "Feasibility of CBCT-based dose calculation: Comparative analysis of HU adjustment techniques," Radiotherapy and Oncology **104**(2), 249–256 (2012).

[6] Siewerdsen, J. H., Moseley, D. J., Bakhtiar, B., Richard, S., Jaffray, D. A., "The influence of antiscatter grids on soft-tissue detectability in cone-beam computed tomography with flat-panel detectors," Medical Physics **31**(12), 3506–3520 (2004).

[7] Graham, S. A., Moseley, D. J., Siewerdsen, J. H., Jaffray, D. A., "Compensators for dose and scatter management in cone-beam computed tomography," Medical Physics **34**(7), 2691–2703 (2007).

[8] Moore, C. J., Marchant, T. E., Amer, A. M., "Cone beam CT with zonal filters for simultaneous dose reduction, improved target contrast and automated set-up in radiotherapy," Physics in Medicine and Biology **51**(9), 2191–2204 (2006).

[9] Rinkel, J., Gerfault, L., Estve, F., Dinten, J.-M., "A new method for x-ray scatter correction: first assessment on a cone-beam CT experimental setup," Physics in Medicine and Biology **52**(15), 4633–4652 (2007).

[10] Siewerdsen, J. H., Daly, M. J., Bakhtiar, B., Moseley, D. J., Richard, S., Keller, H., Jaffray, D. A., "A simple, direct method for x-ray scatter estimation and correction in digital radiography and cone-beam CT," Medical Physics **33**(1), 187–197 (2006).

[11] Poludniowski, G., Evans, P. M., Hansen, V. N., Webb, S., "An efficient Monte Carlo-based algorithm for scatter correction in keV cone-beam CT," Physics in Medicine and Biology **54**(12), 3847–3864 (2009).

[12] Poludniowski, G. G., Evans, P. M., Webb, S., "Cone Beam Computed Tomography Number Errors and Consequences for Radiotherapy Planning: An Investigation of Correction Methods," International Journal of Radiation Oncology*Biology*Physics **84**(1), e109–e114 (2012).

[13] Zijtveld, M. van., Dirkx, M., Heijmen, B., "Correction of conebeam CT values using a planning CT for derivation of the dose of the day," Radiotherapy and Oncology **85**(2), 195–200 (2007).

[14] Hatton, J., McCurdy, B., Greer, P. B., "Cone beam computerized tomography: the effect of calibration of the Hounsfield unit number to electron density on dose calculation accuracy for adaptive radiation therapy," Physics in Medicine and Biology **54**(15), N329 (2009).

[15] Richter, A., Hu, Q., Steglich, D., Baier, K., Wilbert, J., Guckenberger, M., Flentje, M., "Investigation of the usability of conebeam CT data sets for dose calculation," Radiation Oncology **3**(1), 1 (2008).

[16] Fortunati, V., Verhaart, R. F., Angeloni, F., Lugt, A. van der., Niessen, W. J., Veenland, J. F., Paulides, M. M., Walsum, T. van., "Feasibility of Multimodal Deformable Registration for Head and Neck Tumor Treatment Planning," International Journal of Radiation Oncology*Biology*Physics **90**(1), 85–93 (2014).

[17] Fan, Q., Lu, B., Park, J. C., Niu, T., Li, J. G., Liu, C., Zhu, L., "Image-domain shading correction for cone-beam CT without prior patient information," Journal of Applied Clinical Medical Physics **16**(6) (2015).

[18] Marchant, T. E., Moore, C. J., Rowbottom, C. G., MacKay, R. I., Williams, P. C., "Shading correction algorithm for improvement of cone-beam CT images in radiotherapy." Physics in Medicine and Biology **53**(20), 5719–5733 (2008).

[19] Yoo, T. S., Ackerman, M. J., Lorensen, W. E., Schroeder, W., Chalana, V., Aylward, S., Metaxas, D., Whitaker, R., "Engineering and algorithm design for an image processing Api: a technical report on ITK–the Insight Toolkit."

Studies in health technology and informatics **85**, 586–592 (2002).

[20] Joshi, K. D., Marchant, T. E., "Fast processing of CBCT to improve delivered dose assessment," MICCAI ICART workshop (2015).

[21] Leys, C., Ley, C., Klein, O., Bernard, P., Licata, L., "Detecting outliers: Do not use standard deviation around the mean, use absolute deviation around the median," Journal of Experimental Social Psychology **49**(4), 764–766 (2013).

[22] Marchant, T. E., Joshi, K. D., Moore, C. J., "Shading correction for cone-beam CT in radiotherapy: Validation of dose calculation accuracy using clinical images," proc. SPIE Medical Imaging 2017: Physics of Medical Imaging (2017).

APPENDIX A. XVI 5 IMAGES

In a recent update to the Elekta XVI software (XVI 5.0) a correction is applied to the CBCT images during reconstruction. The effect of the correction is similar to global linear scaling applied in the shading correction.

Fig. 12 shows examples of pelvis images acquired using versions 4.5 and 5.0 of the XVI software. One slice of each image is shown, using the same window and level settings.

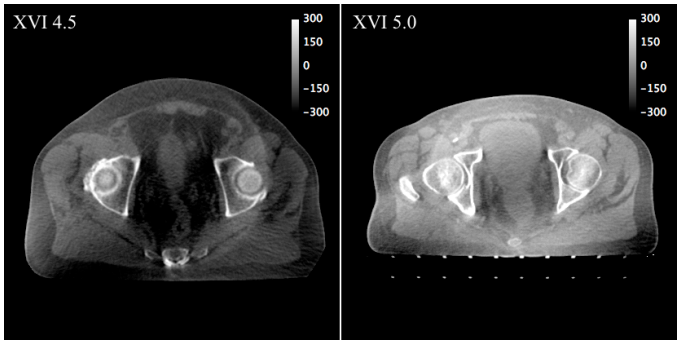

Figure 12. A comparison of pelvis images acquired with versions 4.5 (left) and 5.0 (right) of the Elekta XVI software.

It is clear that the image acquired using XVI 5.0 has pixels with different greyscale values than those in the XVI 4.5 image. The pixels in the XVI 5.0 image more accurately represent Hounsfield Units. This is confirmed by comparing the histograms of the two images, shown in Fig. 13. The entire image volumes are used to populate the histograms, rather than just the single slice of the volumes shown in Fig. 12.

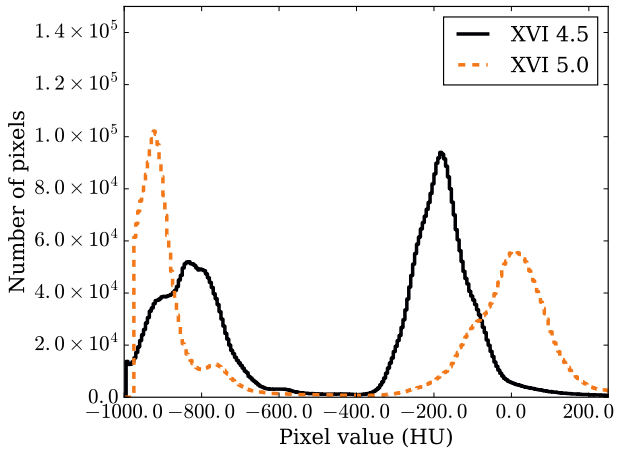

Figure 13. Histograms created using XVI 4.5 (black, solid) and XVI 5.0 (orange, dashed) pelvis images volumes. A single slice of each volume is shown in Fig. 12.

Both histograms exhibit the features present in typical histograms of CBCT images; two main peaks are visible which correspond to pixels representing air (peak with lower pixel values) and soft tissue (higher pixel values). The histogram of the XVI 5.0 image contains air pixels with values closer to the HU definition of -1000, and soft tissue pixels with values closer to the average HU value of tissue, of approximately zero.

Fig. 14(a) and (b) show comparisons of CT and CBCT image histograms corresponding to the XVI 4.5 and XVI 5.0 pelvis images shown in Fig. 12. Histograms created using the corresponding planning CT scans for each pelvis patient are shown in black. They have significantly more detail that the histograms from the unprocessed CBCT images. In particular the CT image histograms have sufficient detail that peaks representing both fat and muscle tissue can be distinguished from each other, at around -50 and +50 HU respectively.

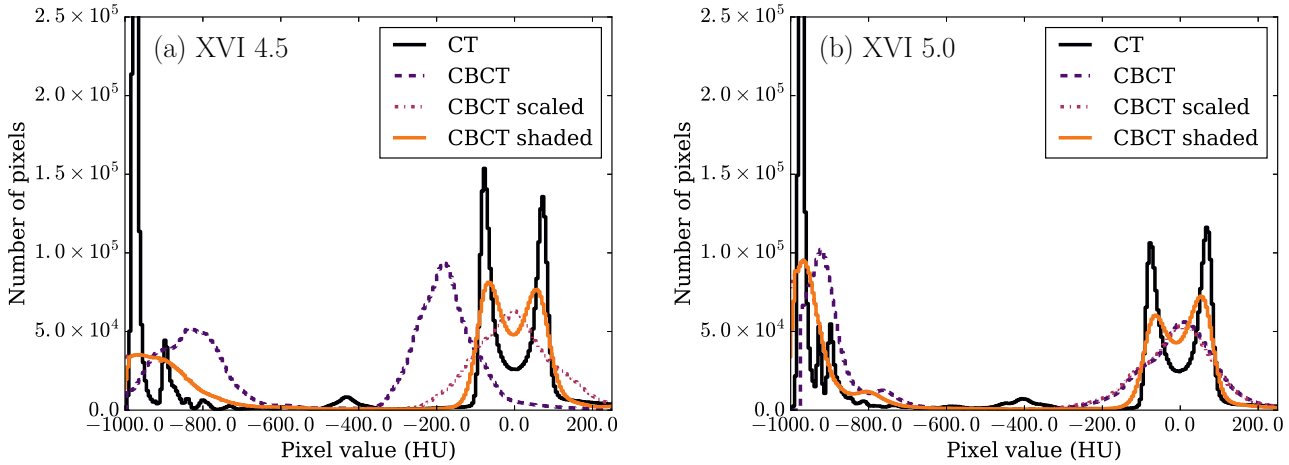

Figure 14. Histograms of CT and CBCT images of the XVI 4.5 (a) and XVI 5.0 (b) pelvis patients. "CT" histograms (black, solid) are created using the patient's corresponding planning CT image. "CBCT" histograms (purple, dashed) are created using the unprocessed CBCT images of the patient. "CBCT scaled" (pink, dot-dashed) histograms are created using CBCT images after the application of the global linear scaling applied as part of the shading correction algorithm. "CBCT shaded" histograms (orange, solid) are created using CBCT images that have been corrected using the full shading correction algorithm.

For the XVI 4.5 image (Fig. 14(a)), the unprocessed CBCT image histogram (purple, dashed) has air and tissue peaks that are offset from the corresponding peaks in the CT image. The application of the global linear scaling corrects this, resulting in an image with pixel values that more closely resemble Hounsfield Units, and a histogram (pink, dot-dashed) that has peaks in the correct locations. The full shading correction further improves the image quality, and the histogram (orange, solid) of the resulting image exhibits separated peaks of fat and muscle tissue, as are present in the original CT image histogram.

The histogram of the uncorrected XVI 5.0 CBCT image (Fig. 14(b), purple, dashed) has air and tissue peaks that are already in approximately the correct location. The global linear scaling applied to the uncorrected XVI 5.0 CBCT image has only a small effect. The position of the air peak in the "CBCT scaled" histogram (pink, dot-dashed) is shifted to be more consistent with the main air peak in the CT image histogram, and the tissue peak is left almost unchanged. However the application of the full shading correction still produces an improvement, and the resulting "CBCT shaded" image histogram (orange, solid) contains the separated fat and muscle tissue peaks that are shown in the corresponding CT image.